ORIGINAL RESEARCH

Single-ended protection method for hybrid HVDC transmission line based on transient voltage characteristic frequency band

Hongchun Shu[1], Shixin Wang[1] and Shunguang Lei[2*]

Abstract

Hybrid high-voltage direct current (HVDC) transmission has the characteristic of long transmission distance, complex corridor environment, and rapid fault evolution of direct current (DC) lines. As high fault current can easily cause irreversible damage to power devices, rapid and reliable line protection and isolation are necessary to improve the security and reliability of hybrid HVDC transmission system. To address such requirement, this paper proposes a single-ended protection method based on transient voltage frequency band characteristics. First, the frequency characteristics of the smoothing reactor, DC filter, and DC line are analyzed, and the characteristic frequency band is defined. A fault criterion is then constructed based on the voltage characteristic frequency band energy, and faulty pole selection is performed according to the fault voltage characteristic frequency band energy ratio. The proposed protection method is verified by simulation, and the results show that it can rapidly and reliably identify internal and external faults, accurately select faulty poles without data communication synchronization, and has good fault-resistance and anti-interference performance.

Keywords Boundary frequency characteristics, Characteristic frequency band, Hybrid HVDC, Single-end protection, Transient voltage

1 Introduction

In China, the main renewable power resources are inversely distributed with the electricity consumption load, while high-voltage direct current (HVDC) transmission is characterized by high transmission capacity, long distance, and narrow transmission corridor [1, 2]. Consequently, HVDC transmission has become an important means of long-distance high-capacity transmission, urban grid expansion, asynchronous grid interconnection, isolated island networking, and new energy

generation delivery, occupying an important position in the modern power system. Therefore, the safe and stable operation of HVDC transmission system is very important to the reliability of the power grid [3, 4]. Line commutated converter-based HVDC (LCC-HVDC) system has the advantages of large capacity, high voltage level, and mature technology. However, LCC is prone to commutation failure, and the ability of an alternating current (AC) system to handle faults is weak [5, 6]. In contrast, modular multi-level converter-based HVDC (MMC-HVDC) system does not require reactive power compensation and has flexible control. Consequently, the LCC-MMC–Hybrid HVDC, which adopts the LCC topology at the transmitter side and the MMC topology at the receiver side [7–10], has the advantages of large transmission capacity, flexible control, no commutation failure risk, and low cost. However, faults on LCC-MMC–Hybrid HVDC transmission lines pose severe

*Correspondence:
Shunguang Lei
leishunguang@hit.edu.cn
[1] Yunnan Key Laboratory of Green Energy, Electric Power Measurement Digitalization, Control and Protection, Kunming University of Science and Technology, Kunming 650500, Yunnan Province, China
[2] School of Electrical Engineering and Automation, Harbin Institute of Technology, Harbin 150001, Heilongjiang Province, China

Shu *et al. Protection and Control of Modern Power Systems*   (2023) 8:26

Page 2 of 11

threats to its safe operation. Thus, it is essential to design suitable line protection for such systems.

DC line fault detection methods can be roughly divided into single- and double-ended methods [11]. The high controllability and vulnerability of a converter bring strict requirements for the operation speed of relay protection, so boundary characteristics-based protection has become a hot research topic in recent years [12]. The boundary characteristics are that when a fault occurs on the different side of a point, the fault characteristics measured at the measuring points are noticeably different. The equipment or a structure with the boundary characteristic is called a boundary [13–16]. In addition, single-terminal protection has the advantage of fast operation and can be used as the main protection type for an HVDC transmission system. In an LCC-HVDC system, single-ended traveling wave protection has been generally used as the main line protection. For instance, ABB uses the variation amount and rate of a voltage traveling wave to construct the main criterion for traveling wave protection to achieve reliable identification of internal and external faults, whereas Siemens used the voltage change and the voltage change rate to construct the protection criterion. Most existing single-ended protection methods adopt a single-ended protection strategy based on high-frequency transient voltage (or current), which can improve the robustness against high transition resistance. The above-mentioned protection criteria use the blocking effect of filters at both ends of a transmission line on the traveling wave to identify internal and external faults. However, no DC filter is installed in a flexible DC transmission system, while flat wave reactors are placed at both ends of a DC line. This can effectively block the traveling wave propagation. Thus, the single-terminal protection principle based on the boundary characteristic can be applied to a flexible DC transmission system [17].

In [15], a protection method based on the transient energy ratio is proposed using the impedance frequency characteristics of a line boundary. In the case of internal faults, the transient energy in a specific frequency band on the line side of a boundary is much larger than that on the valve side. However, for a fault outside the rectifier terminal (i.e., at the inverter terminal), the transient energy on the line side of the rectifier terminal boundary is much smaller than that on the valve side. In [18], the value of the measured surge impedance at the resonant frequency is used for fault identification based on the amplitude-frequency characteristics of a DC filter, though this method has weak robustness to high resistance. By analyzing the wave impedance frequency characteristics of a flat-wave reactor, DC filter, and DC line of the converter station, reference [19] identifies the

internal and external faults based on the difference in the wave impedance amplitude of boundary elements during the internal and external faults. However, this protection method requires a relatively high sampling frequency. In [20], a traveling wave protection scheme for two-terminal LCC-HVDC transmission lines is proposed. However, this method has poor robustness against transition resistance.

To address the shortcomings and limitations of the existing solutions, this paper presents a hybrid HVDC line protection scheme based on the transient voltage characteristic band. First, the rectifier side line boundary and frequency characteristics of a DC line boundary are analyzed. The results indicate that the boundary faults of a high-frequency transient signal have an obvious attenuating effect. According to the rectifier side frequency characteristic line boundary and DC line boundary, the characteristic frequency band is defined, and the characteristics of the frequency band energy of the fault transient voltage signal are determined. The characteristic frequency band energy ratio of the fault voltage transient signal is then used to perform faulty pole selection.

The main contributions of this study can be summarized as follows:

(i)   The boundary frequency characteristics of a hybrid HVDC transmission system are analyzed.
(ii) The feasibility of the proposed method for a hybrid HVDC transmission system is proven theoretically.
(iii) The proposed method is implemented in a protection device and verified in a real project-based PSCAD test system.

2 LCC-MMC–hybrid HVDC topology and self-clearing strategy

2.1 LCC-MMC topology

The topology of the LCC-MMC–Hybrid HVDC transmission system is shown in Fig. 1. It includes an AC transmitter system, an AC receiver system, AC filters,
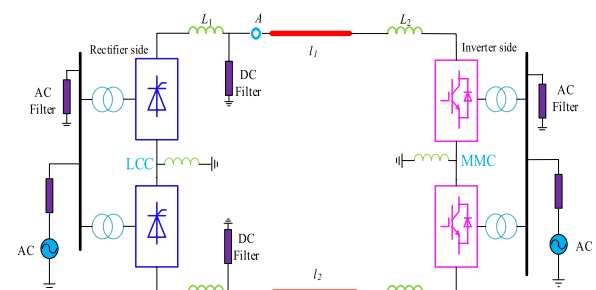
Fig. 1 Topological structure of an LCC-MMC-Hybrid HVDC transmission system

a rectifier side converter, an inverter side converter, flat wave reactors, and DC filters. The rectifier adopts a double 12-pulse LCC converter configuration, and the inverter includes a bipole MMC converter with a full-bridge and half-bridge sub-module hybrid structure. In Fig. 1, *A* denotes the voltage measuring point.

2.2 LCC-MMC self-clearing strategy

In practical applications, half-bridge sub-module MMC converters have been commonly used, but they do not have fault self-clearing capability. Thus, it is necessary to install DC circuit breakers to isolate line faults. However, because of power electronics constraints, existing DC circuit breakers cannot achieve isolation of high-capacity, high-current DC transmission system faults. Therefore, to realize flexible DC high-capacity transmission, the Kun-Liu-Long hybrid HVDC transmission project adopts a full-half hybrid MMC topology at the receiving end, as shown in Fig. 2. This topology enables self-clearing of faults so does not require the installation of DC circuit breakers. When a fault occurs in a DC line, the full-bridge sub-modules will enter the negative state, and the MMC upper and lower arms form a clamp voltage to inhibit fault current development. Therefore, in this study, the forward external fault can be completed by the MMC self-clearing strategy for fault isolation, and only the rectifier-side external fault and line fault are analyzed.

3 Boundary characteristics analysis of hybrid HVDC transmission system

3.1 Rectifier-side line boundary frequency characteristics analysis

Since in this study, an LCC converter station is used at the sending end, which causes large DC output harmonics, a flat-wave reactor and two sets of triple-tuned DC filters are configured at the outlet of the LCC converter station, forming the physical boundary of the rectifier-side line, as shown in Fig. 3.
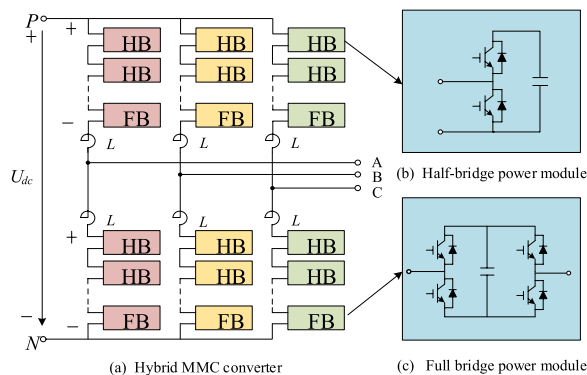
Fig. 2 The topology of a full-half hybrid sub-module MMC
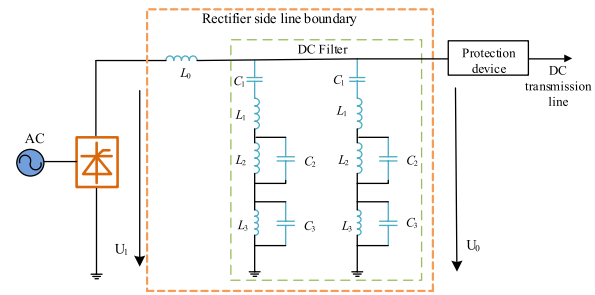
Fig. 3 The rectifier side line boundary

In this study, a 200 mH flat wave reactor is installed at each LCC converter pole and a 150 mH dry flat wave reactor is also installed at the neutral bus. Thus, the total flat wave reactor of a single pole at rectifier side line boundary is 350 mH. The impedance of the flat wave reactor can be expressed as:

$$Z_1 = j\omega L_0 \tag{1}$$

For the DC filters, its configuration is considered to include two groups of three tuned filters per pole, as shown in Fig. 3. Its parameters are: $C_1 = 1.2$ μF, $L_1 = 24.496$ mH, $C_2 = 3.361$ μF, $L_2 = 13.84$ mH, $C_3 = 4.355$ μF, and $L_3 = 2.747$ mH. The equivalent impedance of the DC filter can be expressed as:

$$Z_2 = \frac{1}{2}\left[\frac{1}{j\omega c_1} + j\omega L_1 + \frac{\omega L_2}{j(\omega^2 L_2 c_2 - 1)} + \frac{\omega L_3}{j(\omega^2 L_3 c_3 - 1)}\right] \tag{2}$$

In this paper, the post-fault energy is extracted based on the single-ended voltage value, and the transfer function of the transmission line boundary at the sending end is obtained using U_0 over U_1, where U_1 denotes the voltage on the commutator side of the flat-wave reactor, and U_0 represents the voltage on the line side of the flat-wave reactor. This can be expressed by:

$$G(j\omega) = \frac{U_0}{U_1} \tag{3}$$

In the condition of an open DC line, the transfer function of the rectifier side line boundary can be derived from (3) as:

$$G(j\omega) = \frac{Z_2}{Z_2 + Z_1} \tag{4}$$

After substituting the parameters into (4), the frequency decay characteristics of a rectifier-side line boundary frequency characteristic transfer function $G(j\omega)$ can be obtained, as shown in Fig. 4.

Fig. 4 The rectifier side line boundary frequency characteristics

Fig. 5 The frequency characteristics of a DC line
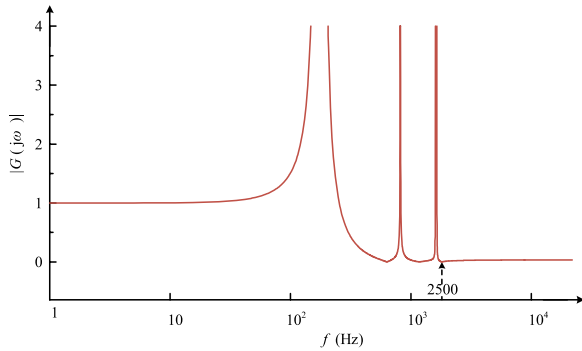
The natural physical boundary of a rectifier-side line consisting of a flat wave reactor and a DC filter can be observed in Fig. 4, as:

- when $0 < f < 100$ Hz, $|G(j\omega)| \approx 1$;
- when 75 Hz $< f < 231$ Hz, $|G(j\omega)| > 1$;
- when $f = 169$ Hz, $f = 475$ Hz, $f = 979$ Hz, and $f = 1562.5$ Hz, $|G(j\omega)|$ takes extremely large value; and
- when $f > 2500$ Hz, $|G(j\omega)| << 1$.

These results indicate that the rectifier side line boundary has a significant attenuation effect on the high-frequency signal of the fault voltage.

3.2 DC line frequency characteristics analysis

The proposed model represents a symmetric bipole DC system, which needs to decouple the positive and negative fault information. Equation (5) is used to decouple the line mode component and the ground mode component, and can be expressed by:

$$D = \frac{1}{\sqrt{2}} \begin{pmatrix} 1 & 1 \\ 1 & -1 \end{pmatrix} \tag{5}$$

When a fault occurs on a DC line, the fault traveling wave is transmitted from the fault point to the converter stations on both sides of the line. Defining the traveling wave voltage of a fault point at any position of a line $U_i(x,s)$ and the traveling wave voltage of the measurement point at the converter terminal as $U_i(0,s)$, the traveling wave voltage at the converter measurement point can then be expressed as:

$$U_i(0,s) = e^{-\gamma_i(s)x} U_i(x,s) \tag{6}$$

where x is the fault distance and $\gamma i(s)$ is the line propagation coefficient.

To study the line fault voltage energy attenuation, $s = j\omega$ is substituted into (6), which yields:
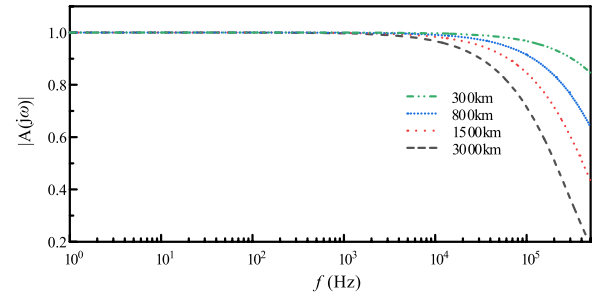
$$\begin{cases} \gamma_i(s) = \sqrt{(r_a + j\omega l_a)(g_a + j\omega c_a)} = \alpha(\omega) + j\beta(\omega) \\ \alpha(\omega) = \sqrt{\dfrac{1}{2\left[r_a g_a - \omega^2 l_a c_a + \sqrt{(r_a^2 + \omega^2 l_a^2)(g_a^2 + \omega^2 c_a^2)}\right]}} \\ \beta(\omega) = \sqrt{\dfrac{1}{2\left[\omega^2 l_a c_a - r_a g_a + \sqrt{(r_a^2 + \omega^2 l_a^2)(g_a^2 + \omega^2 c_a^2)}\right]}} \end{cases} \tag{7}$$

where $\alpha(\omega)$ is the attenuation coefficient and $\beta(\omega)$ is the phase shift coefficient. r_a, l_a, g_a, and c_a are the unit resistance, inductance, conductance, and capacitance of the line, respectively.

Then, the voltage relationship between the fault point and the measurement point can be determined by:

$$U_i(0,s) = e^{-(\alpha(\omega)+j\beta(\omega))x} U_i(x,s) \tag{8}$$

According to (8), the voltage at the fault point in the zone is affected by the fault distance and frequency, and attenuation occurs in the transmission of the line. The frequency attenuation characteristics are shown in Fig. 5.

As shown in Fig. 5, the attenuation of the fault voltage energy of a DC transmission line is related to the length and frequency of the transmission line. That is the frequency attenuation of the DC transmission line mode voltage increases with both the transmission line length and the transmission frequency. The frequency attenuation characteristics of the DC line in Fig. 5 indicate that the frequency attenuation of the DC line is low before 10 kHz but becomes more severe after 10 kHz.

3.3 Characteristic frequency band definition and selection

According to the frequency characteristics analysis results of the rectifier side line boundary and DC line in Sects. 3.1 and 3.2, the boundary causes differences in the energy between frequency bands of internal and external faults. The rectifier side line boundary has a significant attenuation effect on the high-frequency band. When an internal fault occurs, the fault signal does not pass through the rectifier side line boundary

Shu *et al. Protection and Control of Modern Power Systems*   (2023) 8:26

Page 5 of 11

and thus is not attenuated by this boundary. Therefore, large high-frequency fault signals can be detected by the protection system. When an external fault occurs, the fault signal passes through the line boundary on the rectifier side and is attenuated by this boundary, so only small high-frequency fault components can be detected by the protection system. According to the analysis results of the frequency characteristics of the rectifier side line boundary in Sect. 3.1, the rectifier side line boundary affects the low-frequency conduction. Therefore, when an external fault occurs, the voltage fault components can reach the measurement point through the boundary of the rectifier side. As a result, it cannot form an obvious difference with the fault in the occurrence area. According to the analysis results of the boundary frequency characteristics of a DC line in Sect. 3.2, the DC line has an attenuation effect on the

voltage fault signal, and the fault signal is attenuated by the DC line when internal and external faults occur.

In this paper, a multi-scale decomposition of the voltage fault components is performed using wavelet packets to obtain frequencies of the characteristic frequency bands and their energy values in the 1 ms time window. A dB3 wavelet packet is used to perform five-layer decomposition and 32-scale wavelet packet decomposition for a voltage fault component. The sampling frequency is set to 20 kHz, and the frequency of each scale band is 625 Hz. The frequency band energy statistics are shown in Table 1.

As shown in Fig. 4, when the frequency f is higher than 2500 Hz, the rectifier side line boundary has an attenuation effect on high frequencies, corresponding to the band energy band of E_5 in Table 1. To distinguish the fault types better, E_5-E_{13} are defined as characteristic frequency bands, so E_5-E_{13} are large for an internal fault but small for an external fault. The characteristic frequency band energy ΔE can be obtained by:

$$\Delta E = \sum_{i=5}^{13} E_i \tag{9}$$

Next, the 32-scale wavelet packet decomposition of the transient voltage within 1 ms of the occurrence of the voltage fault component is performed, and the wavelet packet energy within the characteristic frequency bands E_5-E_{13} of different fault types is calculated, as shown in Table 2. The full-band fault transient energy curves for different internal and external fault types are displayed in Fig. 6.

The analysis of the results presented in Table 2 and Fig. 6 shows that:

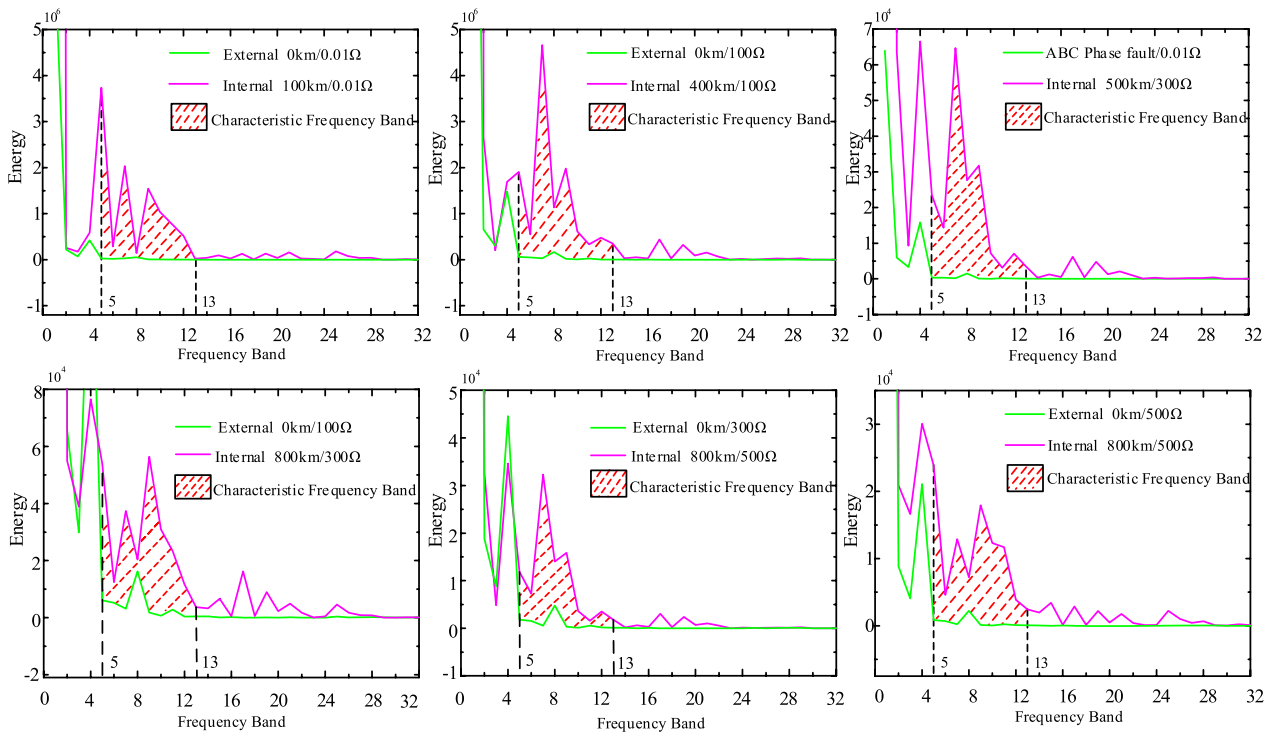(1) When a rectifier-side DC line internal fault occurs, the transient voltage energy of the internal fault

Table 1 The frequency band energy statistics

Energy	Frequency band (Hz)	Energy	Frequency band (Hz)
E_1	0–625	E_{17}	10,000–10,625
E_2	625–1250	E_{18}	10,625–11,250
E_3	1250–1875	E_{19}	11,250–11,875
E_4	1875–2500	E_{20}	11,875–11,250
E_5	2500–3125	E_{21}	11,250–13,125
E_6	3125–3750	E_{22}	13,125–13,750
E_7	3750–4375	E_{23}	13,750–14,375
E_8	4375–5000	E_{24}	14,375–15,000
E_9	5000–5625	E_{25}	15,000–15,625
E_{10}	5625–6250	E_{26}	15,625–16,250
E_{11}	6250–6875	E_{27}	16,250–16,875
E_{12}	6875–7500	E_{28}	16,875–17,500
E_{13}	7500–8125	E_{29}	17,500–18,125
E_{14}	8125–8750	E_{30}	18,125–18,750
E_{15}	8750–9375	E_{31}	18,750–19,375
E_{16}	9375–10,000	E_{32}	19,375–20,000

Table 2 The frequency band energies of different fault types

	Fault type	$E_5/10^5$	$E_6/10^4$	$E_7/10^3$	$E_8/10^4$	$E_9/10^4$	$E_{10}/10^3$	$E_{11}/10^3$	$E_{12}/10^3$	$E_{13}/10^3$	$\triangle E/10^5$
Internal	50 km/0.01 Ω	41.024	66.502	957.341	119.012	136.023	496.435	155.421	535.241	720.412	101.826
	50 km/500 Ω	2.613	2.052	151.214	1.073	10.824	72.262	56.424	34.709	1.971	7.1737
	800 km/0.01 Ω	6.832	7.972	378.346	12.243	15.641	155.364	269.542	26.324	21.424	18.927
	800 km/500 Ω	2.391	4.594	12.943	72.251	1.791	12.324	11.714	3.871	2.416	10.687
External	0.01 Ω	0.267	1.983	31.421	5.424	0.715	2.731	9.099	0.013	3.828	1.551
	500 Ω	0.084	0.007	0.227	0.223	0.011	0.033	0.021	0.010	0.048	0.112
	A phase fault to ground/0.01 Ω	0.005	0.031	0.011	0.007	0.002	0.006	0.001	0.002	0.010	0.009
	AB phase fault to ground/500 Ω	0.011	0.095	0.277	0.032	0.001	0.044	0.032	0.014	0.006	0.028
	ABC phase fault/0.01 Ω	0.032	0.035	0.171	0.149	0.009	0.415	0.218	0.208	0.339	0.065

Fig. 6 Comparison results of the transient voltage energy for different fault types

decreases but is greater in the characteristic frequency bands E_5–E_{13}.

(2) When a rectifier side DC line external fault occurs, compared to the internal fault, the difference in the transient voltage energy is large, especially in the characteristic frequency bands E_5–E_{13}.

The results are consistent with those from the aforementioned analysis of the frequency characteristics of the rectifier-side line boundary and DC line.

4 Graph boundary characteristics analysis of hybrid HVDC transmission system

4.1 Protection activation criterion
Here, the transient voltage characteristic band energy is used to construct a start-up criterion as follows:

$$\Delta E > \Delta E set \tag{10}$$

To avoid the maloperation of AC fault protection, this study uses the AC occurrence of a three-phase metallic fault as a reference value with a 10% margin. $\triangle E_{set}$ is set to 3.3×10^3, which can improve the protection reliability.

4.2 Fault identification criterion
Based on the rectifier side boundary and line frequency characteristics, the internal fault characteristic band energy is much larger than that of the external fault. Therefore, the

difference in the fault characteristic band energy between internal and external faults can be used to construct the protection criterion.

Internal and external fault identification criteria are expressed as follows:

$$\begin{cases} \Delta E > K_{set} \text{ Internal Fault} \\ \Delta E \leq K_{set} \text{ External Fault} \end{cases} \tag{11}$$

where K_{set} is the threshold value. The valve-side metallic fault is used as a base value with a 20% margin, so K_{set} is set to 1.861×10^5.

4.3 Faulty pole identification criterion
According to the voltage characteristics analysis [13], when a pole-to-pole fault occurs, the fault circuit is symmetric and the positive and negative transient voltages are equal. Under a pole-to-ground fault, the fault pole transient voltage is higher than the sound pole transient voltage. Therefore, the characteristic frequency band energy of the positive and negative voltage fault components can be used for fault selection, and the selection criterion can be constructed as:

$$\left\{ F = \sum_{i=5}^{13} E_{i+} \bigg/ \sum_{i=5}^{13} E_{i-} \right. \tag{12}$$

where $\sum\limits_{i=5}^{13} E_{i+}$ and $\sum\limits_{i=5}^{13} E_{i-}$ are the sums of energy of the positive and negative characteristic frequency bands, respectively.

Then, the identification criterion of fault pole selection can be established as:

$$\begin{cases} F > 1.2, & \text{Positive pole fault} \\ F < 0.8, & \text{Negative pole fault} \\ 0.8 \leq F \leq 1.2, & \text{Pole - to - pole fault} \end{cases} \quad (13)$$

For a pole-to-pole fault, F has a value of one, and adopts a 20% margin.

4.4 Protection process

According to the defined fault identification criterion, the fault identification criterion and the faulty pole selection criterion described in Sects. 4.1 to 4.3 are derived. The flowchart of the single-end transient voltage protection method of a hybrid HVDC line based on the characteristic frequency band of the transient voltage is shown in Fig. 7.
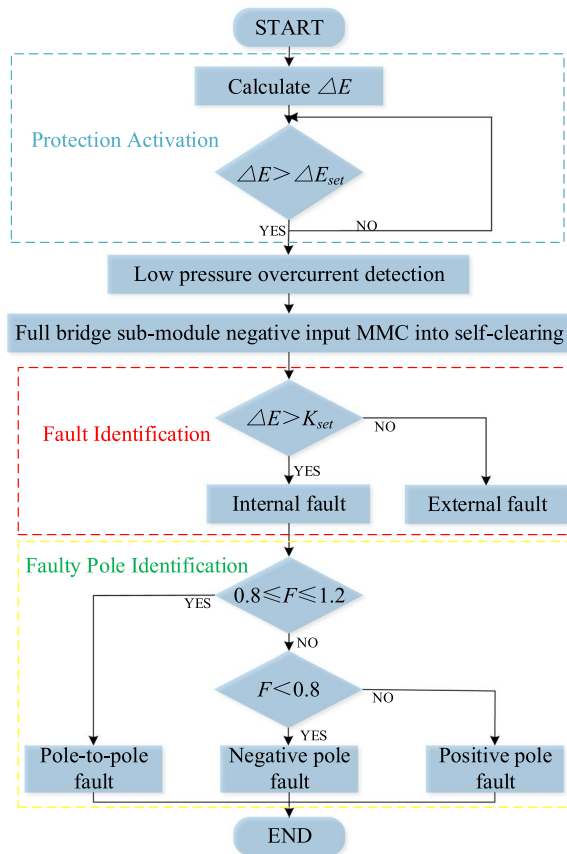
Fig. 7 The flowchart of the proposed protection method

As shown in Fig. 7, the characteristic frequency band energy ΔE is calculated first according to the voltage fault component of the measurement point. When the condition of $\Delta E > \Delta Eset$ is met, the protection method starts. Then, the low-voltage overcurrent detection is performed, the full bridge sub-modules generate negative output, and the MMC enters a self-clearing operation. The condition of $\Delta E > K_{set}$ will be met for an internal fault, whereas the condition $\Delta E < K_{set}$ will be satisfied for an external fault. Finally, fault selection is carried out. If $F > 1.2$ is satisfied, the fault is a positive pole fault, if $F < 0.8$ is satisfied, the fault is a negative pole fault, and if $0.8 \leq F \leq 1.2$ is satisfied, the fault is pole-to-pole fault.

5 Simulation results

5.1 Test system

The hybrid HVDC transmission system model as shown in Fig. 1 is built on the PSCAD platform to verify the proposed protection scheme. The data on 20 points after the fault occurrence are selected, the sampling frequency is 20 kHz, and the data in the 1 ms time window are used. General fault self-clearing in 2 ms is performed after the detection of the fault, and using the 1 ms fault data ensures that the selected data denote the full amount of the fault signal. The simulated system parameters and line parameters are shown in Table 3 and Fig. 8, respectively.
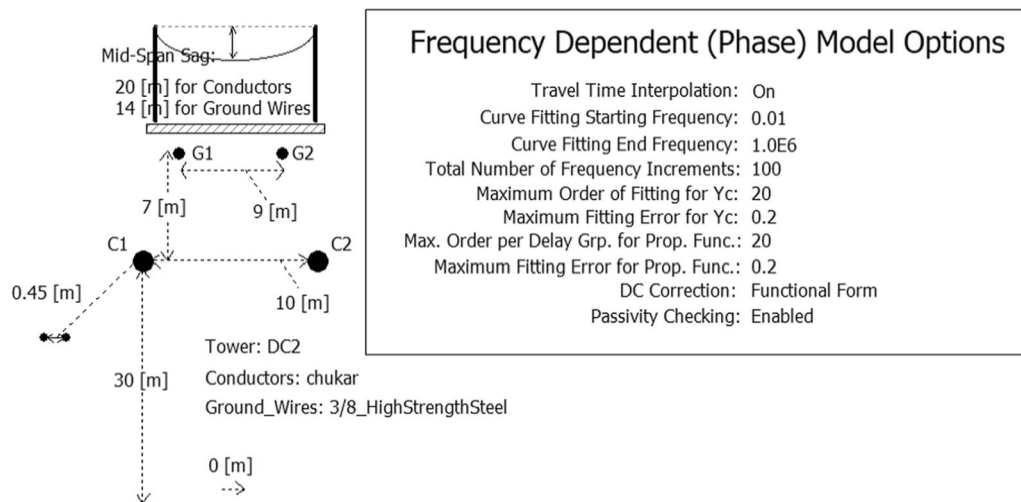
5.2 Different fault type simulation

To verify the adaptability of the proposed protection method to different fault types, the protection algorithm is verified under positive pole internal, negative pole internal, double-zone, valve side, and AC three-phase faults. The discriminant results are shown in Table 4.

As presented in Table 4, when internal faults occur, including positive, negative, and pole-to-pole faults, the energy of the characteristic frequency band is much

Table 3 Simulation system parameters

	Parameter	Value
System	Rated power (MVA)	8,000
	Rated DC voltage (kV)	±800
	Rated DC current (kA)	5
	Sampling frequency (kHz)	20
LCC	AC system voltage (kV)	545
	Flat wave reactor (mH)	200
MMC	AC system voltage (kV)	230
	Flat wave reactor (mH)	75
	Number of bridge arm sub-modules	100
	Sub-module capacitance (mF)	10
	Bridge arm inductor (mH)	200

Fig. 8 Illustration of the transmission line frequency variable parameter model and tower model

Table 4 Simulation results for different fault types

Fault type	Transition resistance (Ω)	Fault distance (km)	$\Delta E(10^5)$	F	Discriminatory result
Positive pole fault	0.01	800	18.9	1.79	Positive pole fault
Negative pole fault	0.01	800	18.1	0.56	Negative pole fault
Pole-to-pole fault	0.01	800	132	1.04	Pole-to-pole fault
External fault	0.01	0	1.55	–	External fault
AC fault	0.01	–	0.03	–	External fault

higher than that of the valve-side and AC faults. This demonstrates that the proposed protection method shows obvious differences in results, and it is easy to identify both internal and external faults and determine the fault poles.

5.3 Different fault distance simulation

Considering the attenuation effect of a long line on the high-frequency energy of the fault voltage, the attribute of fault on the valve side is similar to the line fault, and it is difficult to distinguish between them. In this study, the ΔE values of full-length positive pole fault, valve side positive pole fault, and three-phase fault are compared with a fault resistance of 0.01 Ω. The simulation results are shown in Table 5 and Fig. 9.

From the results in Table 5 and Fig. 9, the characteristic frequency band energy of an internal fault decreases with the fault line length, but it is still significantly different from the valve side fault and AC three-phase fault in numerical value. Thus, the proposed protection method based on the characteristic frequency band can identify the internal and external faults under different fault distances, and the fault criterion is obvious.
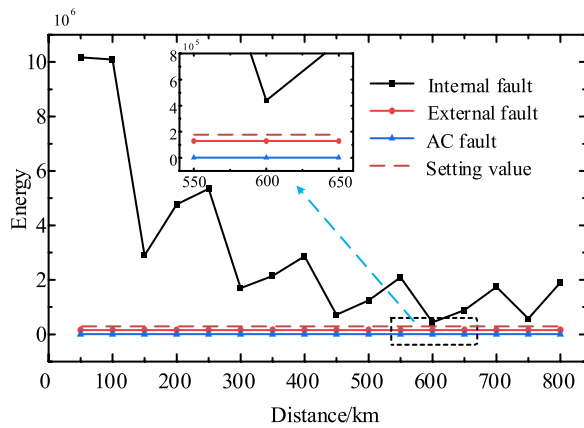
Table 5 Simulation results for different fault distances

Fault type		Fault distance (km)	$\Delta E/10^5$
Internal fault/0.01 Ω		50	102
		100	101
		200	47.8
		300	17.0
		400	28.7
		500	12.4
		600	11.6
		700	10.4
		800	6.80
External fault	0.01Ω	–	1.55
	ABC Phase fault	–	0.006

5.4 Different fault resistance simulation

To verify the ability of the proposed protection method for varying fault resistances, DC line faults with fault resistances of 0.01 Ω, 100 Ω, 300 Ω, and 500Ω are analyzed. The fault distance is set to 100 km, and the verification results are shown in Table 6.

Fig. 9 Comparison results for different fault distances for internal and external faults
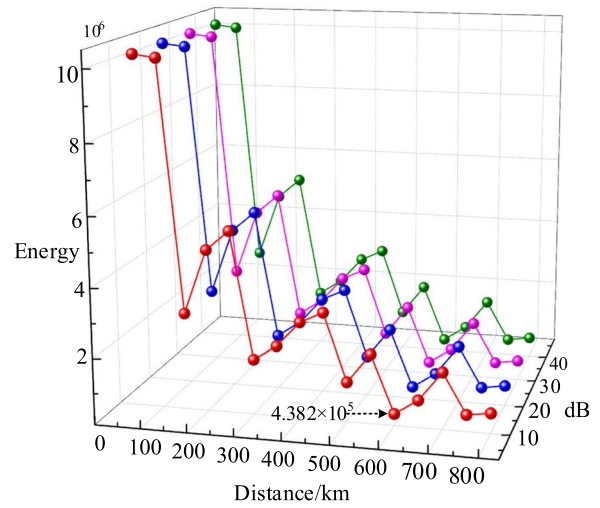

Fig. 10 Simulation results after adding SNR to the internal faults

Table 6 Simulation results for different fault resistances

Fault type	Fault resistance (Ω)	$\Delta E/10^4$
Internal fault/50 km	0.01	1012
	100	420
	300	144
	500	71.7
External fault/0 km	0.01	15.5
	100	3.69
	300	9.81
	500	4.50
External A phase fault	0.01	0.030
	100	0.002
	300	0.001
	500	0.001

As can be seen from Table 6, the energy of the characteristic frequency band decreases with the fault resistance. The characteristic band energy of the internal fault is 71.7×10^4 when the fault resistance is 500 Ω, whereas the characteristic frequency band of the external fault with 0.01 Ω fault resistance is 15.5×10^4. Under the 500 Ω fault resistance, the characteristic frequency bands of the internal and external faults differed significantly, so the faults inside and outside the zone can be effectively identified. It proves that the method has strong ability to withstand fault resistance variation.

5.5 Anti-interference capability analysis
To verify the anti-SNR interference capability of the proposed protection method, SNR of 10 dB, 20 dB, 30 dB, and 40 dB are added to the internal and external faults in turn. The results for the internal and external faults are shown in Fig. 10 and Table 7.

From the results presented in Fig. 10 and Table 7, the characteristic band energy only sees small changes under SNR of 10–40 dB. The minimum value of the internal fault characteristic band energy is 4.382×10^5, while the maximum value of the external fault characteristic band energy is 1.547×10^5. This can meet protection calibration requirements. The protection scheme can resist the 10 dB SNR interference and has a strong anti-interference capability.

5.6 Comparison with other protection methods
To illustrate the contribution and innovation of this study, the proposed method is compared with several existing protection methods.

(1) The fault resistance of the proposed method is compared with those of the existing methods, and the results are presented in Table 8. It can be seen that the proposed method is effective and has good robustness in the case of a high fault resistance.
(2) The robustness of the proposed method against noise interference is compared with those of the existing methods, and the results are presented in Table 9. It can be seen that the proposed method is effective even under an SNR of 10 dB, validating that the proposed method has a strong anti-noise capability.

6 Conclusion
This paper proposes a single-end protection method for hybrid HVDC transmission lines based on the characteristic frequency band of transient voltage. The frequency

Table 7 Simulation results obtained after adding SNR to the external faults

Fault type	Fault resistance (Ω)	SNR			
		10 dB	20 dB	30 dB	40 dB
External fault (0 km)	0.01	1.546×10^5	1.546×10^5	1.547×10^5	1.546×10^5
	100	3.700×10^4	3.693×10^4	3.688×10^4	3.690×10^4
	300	9.865×10^3	9.826×10^3	9.794×10^3	9.806×10^3
	500	4.502×10^3	4.498×10^3	4.493×10^3	4.496×10^3
ABC phase fault	0.01	3.733×10^3	3.628×10^3	3.644×10^3	3.644×10^3
	100	1.352×10^2	1.613×10^2	1.591×10^2	1.569×10^2
	300	4.082×10^1	3.501×10^1	3.140×10^1	3.203×10^1
	500	2.316×10^1	1.533×10^1	1.476×10^1	1.499×10^1

Table 8 Comparison results of different methods with different fault resistance

Method	Fault resistance (Ω)			
	100	200	300	500
Ref. [20]	√	√	√	✕
Ref. [21]	√	√	√	✕
Ref. [22]	√	√	√	✕
Ref. [23]	√	✕	✕	✕
Proposed method	√	√	√	√

Table 9 Simulation results for different SNR

Method	SNR (dB)			
	10	20	30	40
Ref. [24]	✕	✕	√	√
Ref. [25]	✕	✕	✕	√
Ref. [26]	✕	√	√	√
Proposed method	√	√	√	√

characteristics of the smoothing reactor, DC filter, and DC line are studied, and the characteristic frequency band is defined. A fault criterion is constructed based on the voltage characteristic frequency band energy, and the faulty pole selection element is designed using the fault voltage characteristic frequency band energy ratio. The main conclusions of this study are as follows:

(1) When an internal fault occurs, the fault voltage signal does not pass through the rectifier side of the line boundary, and the fault voltage high-frequency signal is not subjected to the attenuation of the rectifier side of the line boundary. However, under an external fault, the fault voltage high-frequency signal is attenuated by the rectifier side line boundary;

(2) The proposed method uses the transient voltage characteristic band energy to construct the protection criterion, and the criterion is obvious. This method does not require data communication synchronization and has high reliability and is fast;

(3) Numerous simulation results show that the proposed protection method can identify faults within 1 ms, cope with a 500 Ω fault resistance, and resist noise interference with SNR of 10 dB. Compared with the existing methods, the proposed method has better robustness against fault resistance and interference.

Author contributions
HS, provided the idea and other technical guidance required for completing the study. SL, the corresponding author, carried out the protection principle studies, revise the manuscript. SW, he completed practical design, case study and drafted the manuscript. All authors read and approved the final manuscript.

Authors' information
Hongchun Shu (1961-), male, PHD and Professor, received his Ph.D. degree in electrical engineering from Harbin Institute of Technology, China, in 1997. He was a professor in 1998 and completed Postdoctoral from Station of Xi'an Jiao Tong University in 1999. He presided over key projects and general projects of National Natural Science Foundation of China, "863" projects, Yunnan science and technology tackling key projects and key fund projects, totaling 13 items. include modular multi-level converter (MMC), HVDC transmission control and protection, transmission line traveling wave fault location.
Shixin Wang (1997-), male, master, studied for a M.S. degree at Kunming University of Science and Technology, Kunming, China, in 2021. His current research interests include key technologies of flexible DC transmission, hybrid multi-terminal DC transmission line protection.
Shunguang Lei (1995-), male, PHD, received the M.S. degree in Kunming University of Science and Technology, Kunming, China, in 2020. He is currently pursuing the Ph.D. degree at Harbin Institute of Technology, Harbin, China. His current research interests include modular multi-level converter (MMC), HVDC transmission control and protection, transmission line traveling wave fault location.

Declarations

References

1. He, J., Chen, K., Li, M., et al. (2020). Review of protection and fault handling for a flexible DC grid. *Protection and Control of Modern Power Systems, 5*(15), 15–29.
2. Lei, S., Shu, H., Li, Z., et al. (2022). A faulty pole detection method for the VSC-HVDC system based on the aperiodic component energy. *Electric Power Systems Research, 212*, 108650.
3. Muniappan, M. (2021). A comprehensive review of DC fault protection methods in HVDC transmission systems. *Protection and Control of Modern Power Systems, 6*(1), 1-19.
4. Agarwala, S., Swetapadmab, A., Panigrahia, C., et al. (2019). A method for fault section identification in High voltage direct current transmission lines using one End measurements. *Electric Power Systems Research, 172*, 140–151.
5. Liu, Z., Gao, H., Luo, S., et al. (2020). A fast boundary protection for an AC transmission line connected to an LCC-HVDC inverter station. *Protection and Control of Modern Power Systems, 5*(29), 29–40.
6. Wang, D., Hou, M., Gao, M., et al. (2020). Travelling wave directional pilot protection for hybrid LCC-MMC-HVDC transmission line. *International Journal of Electrical Power and Energy Systems, 115*, 105431.
7. Zhang, C., Huang, J., Song, G., et al. (2021). Non-unit ultra-high-speed line protection for multi-terminal hybrid LCC/MMC HVDC system and its application research. *IEEE Transactions on Power Delivery, 36*(05), 2825–2838.
8. Chen, X., Li, H., Liang, Y., et al. (2020). A protection scheme for hybrid multi-terminal HVDC networks utilizing a time-domain transient voltage based on fault-blocking converters. *International Journal of Electrical Power & Energy Systems, 118*, 105825.
9. Huang, Q., Zou, G., Wei, X., et al. (2019). A non-unit line protection scheme for MMC-based multi-terminal HVDC grid. *International Journal of Electrical Power & Energy Systems, 107*, 1–9.
10. Shu, H., Lei, S., Tian, X., et al. (2019). A new topology of modular multilevel converter with voltage self-balancing ability. *IEEE Access, 7*, 184786–184796.
11. Li, B., He, J., Li, Y., et al. (2019). A review of the protection for the multi-terminal VSC-HVDC grid. *Protection and Control of Modern Power Systems, 4*(21), 21–31.
12. Duan, J., Li, H., Lei, Y., et al. (2020). A novel non-unit transient based boundary protection for HVDC transmission lines using synchrosqueezing wavelet transform. *International Journal of Electrical Power & Energy Systems, 115*, 105478.
13. Lei, S., Shu, H., Li, Z. (2023). A protection principle of LCC-VSC three-terminal HVdc system based on instantaneous boundary impedance. *IEEE Transactions on Industrial Electronics.* https://doi.org/10.1109/TIE.2023.3260339.
14. Zhang, Y., Li, Y., Song, J., et al. (2019). A new protection scheme for HVDC transmission lines based on the specific frequency current of DC filter. *IEEE Transactions on Power Delivery, 34*(2), 420–429.
15. Dai, Z., Liu, N., Liu, N., et al. (2020). A pilot protection for HVDC transmission lines based on transient energy ratio of DC filter link. *IEEE Transactions on Power Delivery, 35*(4), 1695–1706.
16. Shu, H., Wang, G., Tian, X., et al. (2022). Single-ended protection method of MMC-HVDC transmission line based on random matrix theory. *International Journal of Electrical Power & Energy Systems, 142*, 108299.
17. Zheng, Y., He, J., Li, B., et al. (2021). Research on DC protection strategy in multi-terminal hybrid HVDC system. *Engineering, 7*(8), 1064–1075.
18. Liu, N., Li, Y., Li, S., et al. (2022). A pilot protection for LCC-HVDC transmission lines based on measured surge impedance at tuning frequency. *IEEE Transactions on Power Delivery, 37*(3), 2090–2103.
19. Zhang, D., Wu, C., He, J., et al. (2022). A new protection scheme for transmission line of three-terminal hybrid HVDC system. *International Journal of Electrical Power & Energy Systems, 134*, 107446. https://doi.org/10.1016/j.ijepes.2021.107446.
20. Wu, J., Li, H., & Wang, G. (2017). An improved traveling-wave protection scheme for LCC-HVDC transmission lines. *IEEE Transactions on Power Delivery, 32*(1), 106–116.
21. Song, G., Hou, J., Guo, B., et al. (2020). Pilot protection of hybrid MMC DC grid based on active detection. *Protection and Control of Modern Power Systems, 5*(1), 6–20.
22. Zou, G., Huang, Q., Song, S., et al. (2017). Novel transient-energy-based directional pilot protection method for HVDC line. *Protection and Control of Modern Power Systems, 2*(1), 15–24.
23. Agarwal, S., Swetapadma, A., & Panigrahi, C. K. (2018). An improved method using artificial neural network for fault detection and fault pole identification in voltage source converter-based HVDC transmission lines. *Arabian Journal for Science and Engineering, 43*(8), 4005–4018.
24. Qin, Yu., Wen, M., Zheng, J., et al. (2018). A novel distance protection scheme for HVDC lines based on R-L model. *International Journal of Electrical Power & Energy Systems, 100*, 167–177.
25. Chen, X., Li, H., Wang, G., et al. (2021). A convolution power-based protection scheme for hybrid multiterminal HVDC transmission systems. *IEEE Journal of Emerging and Selected Topics in Power Electronics, 9*(2), 1655–1667.
26. Zheng, J., Wen, M., & Qin, Y. (2020). A novel pilot directional backup protection scheme based on transient currents for HVDC lines. *International Journal of Electrical Power and Energy Systems, 115*, 105424. https://doi.org/10.1016/j.ijepes.2019.105424